Available online at www.sciencedirect.com

ScienceDirect

Procedia CIRP 71 (2018) 466–471

www.elsevier.com/locate/procedia

4th CIRP Conference on Surface Integrity (CSI 2018)

# Experimental and FEM analysis of surface integrity when broaching Ti64

G. Ortiz-de-Zarate[a*], A. Madariaga[a], A. Garay[a], L. Azpitarte[a], I. Sacristan[a,b], M. Cuesta[a], P. J. Arrazola[a]

[a]*Mondragon Unibertsitatea, Faculty of Engineering, Loramendi 4, Arrasate-Mondragón, 20500, Spain*
[b] *AB Sandvik Coromant, Lerkrogsvägen 13, Stockholm, 126 80, Sweden*

* Corresponding author. Tel.: +34 943 79 47 00; fax: +34 943 79 15 36. *E-mail address:* gortizdezarate@mondragon.edu

**Abstract**

The performance of aeronautic critical components is strongly dependent on its fatigue behavior, which is directly linked to their surface integrity condition. Broaching operation is a machining operation extensively used for the manufacturing of some features due to the good dimensional quality and surface integrity condition obtained. Thus, the characteristics of surface integrity obtained in broaching is a key aspect to be considered for the improvement of the fatigue life. This work proposes a Finite Element Method (FEM) model for the prediction of the surface integrity (material damage and residual stresses) of the workpiece obtained after the broaching process using the commercial finite element software DEFORM 2D. The model includes a self-characterized Johnson-Cook flow stress constitutive law for the titanium alloy Ti64. Experimental tests were carried out in an EKIN RAS 10x160x320 hydraulic broaching machine at different cutting conditions for the validation of the predictive model. Apart from the fundamental output variables, such as, forces and chip morphology, a comprehensive study of the surface integrity of the machined piece was done. The residual stresses generated by the cutting process were measured by the hole-drilling technique. Microstructural alterations (material damage) of the workpiece was analyzed by optical microscopy and Scanning Electron Microscope. Finally, the surface topography was examined by contact and optical profilometers. The results of the predictions showed significant good agreement with the experimental tests.


Selection and peer-review under responsibility of the scientific committee of the 4th CIRP Conference on Surface Integrity (CSI 2018).

*Keywords:* Broaching, Surface Integrity, FEM, Ti64

## 1. Introduction

Titanium alloys have received considerable interest recently due to their wide range of applications in aerospace, automotive, chemical and medical industries. The most common titanium alloy is Ti6Al4V (Ti64), which belongs to the α+β alloy group and accounts for more than 50% of the titanium alloy production [1].

Ti64 alloy has been so widely employed due to its low density in combination with high strength at elevated temperatures, as well as, high creep and corrosion resistance [2]. Nevertheless, it has been classified as difficult-to-cut material on account of its poor machinability as a result of its low thermal conductivity, small deformation coefficient and high chemical activity. That properties produce chip-tool adhesion and chip segmentation, making it difficult to ensure the surface integrity condition after the machining process [1,3].

Surface integrity term encompasses material properties (residual stresses, hardness etc.), metallurgical states (phase transformation, microstructure etc.) and topological aspects (roughness etc.). Thus, it is directly related to the quality of the final machined surface, which at the same time is linked to the fatigue life of the piece [4]. Hence, special attention has to be paid during the finishing operation of the pieces since it stablishes the final surface integrity condition of the component.

Broaching is a finishing operation of machining where in a single-pass and using a multiple edged tool high Material Removal Rates (MRR) are reached. All single cutting edges are arranged in a row and each edge is stepped by an offset (rise per tooth) which corresponds to the cutting thickness or feed [5]. It


Selection and peer-review under responsibility of the scientific committee of the 4th CIRP Conference on Surface Integrity (CSI 2018).
10.1016/j.procir.2018.05.033

is widely used in aerospace industry due to the good dimensional quality and surface integrity condition obtained.

Nonetheless, it has barely been studied in comparison to other machining operations, such as turning or milling [4,6]. However, there are some attempts to predict fundamental variables by the Finite Element Method (FEM). Because of the geometrical similarities, all the studied works simplify the broaching process to 2D orthogonal cutting. That is, the analysis was centered in the middle of the slot were plain strain assumption can be done. For instance, Vogtel *et al.* [7] developed a FEM model in DEFORM 2D to predict forces for Inconel 718, so as to reduce the number of experimental tests. Kong *et al.* [8] also developed an orthogonal cutting model in Abaqus 2D for the nickel-based superalloy GH4169 that introduced Johnson-Cook material fracture criteria (without experimental validation). However, none of the works analyzes the titanium alloy Ti64.

Nevertheless, for Ti64 other works were developed for orthogonal cutting and these results may be extrapolated to the broaching operation. Umbrello [9] and Calamaz *et al.* [10] developed FEM models in DEFORM 2D and FORGE respectively. Different flow stress models were used, but both used the Cockroft and Latham's material failure criterion. Calamaz *et al.* obtained the best results with the critical damage value ($D$) of 2400 MPa, while Umbrello with 100-400 MPa. Calamaz *et al*. blamed that difference in critical damage value ($D$) to the mesh size. Nonetheless, both focused on the forces and chip segmentation without analyzing the surface integrity of the machined surface. Moreover, the cutting speed was significantly different from the broaching condition (cutting speeds typically below 20 m/min), since the lowest cutting speed was of 60 m/min.

Childs *et al*. [11] developed a model in AdvantEdge 2D which implements a failure criterion as function of temperature and stress triaxiality for Ti64. The model was calibrated for low cutting speed (below 10 m/min) and then validated at high cutting speed, showing good agreement in force and chip morphology prediction. Moreover, some microstructural changes as surface drag was observed in the machined surface in the experimental and FEM results. However, the surface integrity was beyond the scope of the paper, hence not in depth attention was paid.

To the best of our knowledge, no author has made experimental and FEM analysis of fundamental variables, as well as the surface integrity condition of the workpiece for broaching of Ti64. The paper presents an orthogonal cutting FEM model not only able to predict forces and chip morphology but also residual stresses and material damage in a qualitative way when broaching Ti64. Moreover, experimental analysis was done for the validation of the FEM model in fundamental and surface integrity outputs.

## 2. Finite element model

### *2.1. Input parameters*

For modelling purposes, the reliability of the predictive models are strongly dependent on the flow stress model, thermal characterization of the workpiece and friction model [12,13]. In the present work, the plastic behavior of the material was characterized based on dynamic compression tests. The resultant regression to Johnson-Cook (JC) [14] flow stress law coefficients for the numerical model are given in the Table 1. JC model was slightly modified introducing a cut-off strain of 1 that limits the flow stress above that value, so as to reproduce the strain softening phenomena known to occur in Ti64 alloy. Thermal parameters were obtained from the DEFORM 2D software library and are detailed in Table 1.

Table 1. Input parameters for the FEM model.

| | | |
|---|---|---|
| JC constitutive model | $A$ [MPa] | 1130 |
| | $B$ [MPa] | 530 |
| | $C$ | 0.0165 |
| | $m$ | 0.61 |
| | $n$ | 0.39 |
| | $\dot{\varepsilon}_0$ [$s^{-1}$] | 1 |
| | $T_{room}$ [ºC] | 20 |
| | $T_{melt}$ [ºC] | 1670 |
| Young's modulus, $E$ [GPa] | Ti6Al4V | 117.2 (20ºC) |
| | | 82.7 (650ºC) |
| | HHS (M35) | 205 |
| Poisson's ratio, $v$ | Ti6Al4V | 0.31 |
| | HHS (M35) | 0.3 |
| Density, $\rho$ [kg/m³] | Ti6Al4V | 4430 |
| | HHS (M35) | 8050 |
| Conductivity, $k$ [W/mºC] | Ti6Al4V | 6.9 (20ºC) |
| | | 18 (950ºC) |
| | HHS (M35) | 28 |
| Expansion, $\lambda$ [1/ºC] | Ti6Al4V | 9.1 $e^{-6}$ (20ºC) |
| | | 1.1 $e^{-5}$ (815ºC) |
| | HHS (M35) | 1.16 $e^{-5}$ |
| Specific heat, $c_p$ [J/kgºC] | Ti6Al4V | 520 (20ºC) |
| | | 763 (650 ºC) |
| | HHS (M35) | 926 |
| Cockroft and Latham's material failure | $D$ [MPa] | 200 |
| Friction coefficient | $\mu$ | 0.7 |
| | $m$ | 1 |
| Friction energy to heat [%] | 100 | |
| Inelastic heat fraction | 0.9 | |
| Cutting speed, $V_c$ [m/min] | 2.5 and 7.5 | |
| Feed [mm] | 0.015 | |
| Rake angle, $\gamma$ [°] | 20 | |
| Clearance angle, $\alpha$ [°] | 2 | |
| Cutting edge radius, $r$ [µm] | 10 | |

Furthermore, as followed by other authors in the prediction of chip segmentation in titanium alloy machining, it is necessary to implement a material failure criteria. In this research, Cockroft and Latham's fracture criterion [15] was employed to predict the effect of tensile stress on the chip segmentation (see equation 1). Cockroft and Latham's criterion says that when the integral of the largest tensile principal stress

component over the plastic strain path in Eq. 1 reaches the value of $D$, usually called damage value, fracture occurs or chip segmentation starts.

$$\int_0^{\bar{\varepsilon}_f} \sigma_1 \mathrm{d}\bar{\varepsilon} = \mathrm{D} \quad (1)$$

where, $\bar{\varepsilon}_f$ is the effective strain, $\sigma_1$ the maximum principal stress and $D$ is a material constant.

Finally, as observed by Arrazola and Ozel [16] the friction model highly influences the reliability of the results. Hence, the applied friction law was a sticking-sliding model (see Eq. 2). As observed by Rech *et al.* [17] the sliding velocity is inverse to the friction coefficient, so in the low cutting speeds of the broaching operation significantly high friction coefficients need to be applied. In that sense, in the present simulations $\mu$ value of 0.7 and $m$ of 1 were chosen (see Table 1).

$$\tau = \min\ (\mu \cdot \sigma_n\ , m \cdot k) \quad (2)$$

where, $\tau$ is the friction shear stress, $k$ is the shear yield stress, $\sigma_n$ is the interface pressure and $\mu$, $m$ are friction factors.

### *2.2. FEM model*

The commercial software DEFORM 2D [18], which uses a Lagrangian implicit code was used for the FEM modelling. The software provides robust results without mesh distortion problems and high control of the mesh. The analysis focused on the middle of the slot where plain strain assumption can be done. Hence, a plane strain coupled thermomechanical analysis was performed.

The model consists of a rigid tool and an elastoplastic workpiece, meshed with 2000 and 6000 isoparametric quadrilateral elements respectively. The minimum element size was below 1 µm and maximum was 10 µm. A local remeshing criteria based on strain and strain rate was established. The remeshing technique avoids mesh distortion at large strains, so as to ensure robust results. It also allows maintaining small elements in the cutting area during computing.

The initial geometry of workpiece was a rectangular block (0.5x2.5 mm) of titanium alloy Ti64 fixed in space. The tool moves horizontally from the right to the left at the cutting speed, to remove the upper layer of the workpiece. Fig. 1 shows all the boundary conditions applied to the model.

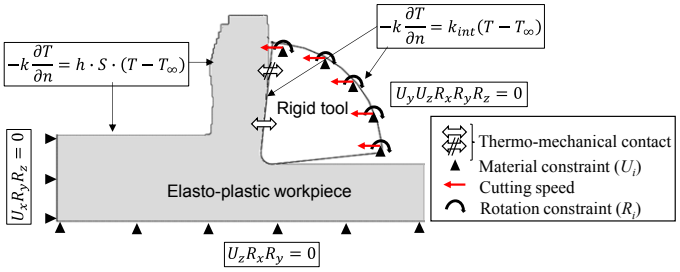


Fig. 1. Boundary conditions of the FEM model.

## 3. Experimental plan

Experimental tests were carried out for the different machining conditions (two cutting speeds). The broaching tests were carried out in an EKIN RAS 10x160x320 hydraulic broaching machine with a Kistler 9255B dynamometer to measure cutting and feed forces (see Fig. 2). A sample rate of 5000 Hz and a 300 Hz cut-off filter was employed. The software Matlab 2017R was used to capture the forces and to filter the signal. To complete the setup, a LVDT sensor was used to obtain the real velocity of the tool.

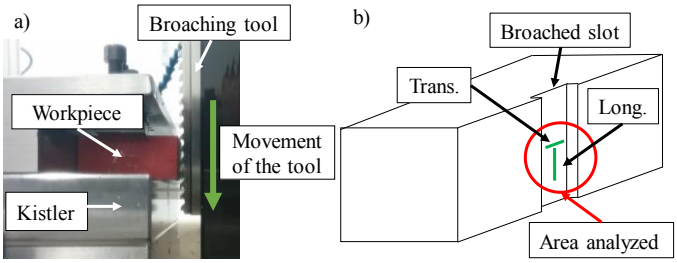


Fig. 2. a) Broaching setup. b) Broached slot.

A rectangular broaching tool was chosen for the experimental tests. Three repetitions were done for each cutting condition, so in total 6 tests were carried out. Table 2 shows the complete experimental plan.

Table 2. Experimental plan.

| | | |
|---|---|---|
| Broaching tool | Material | HSS (M35) |
| | Rake angle, γ [°] | 20 |
| | Clearance angle, α [°] | 2 |
| | Rise per tooth [mm] | 0.015 |
| | Pitch [mm] | 10 |
| | Width [mm] | 10 |
| | Cutting edge radius, $r$ [µm] | 10±2 |
| | Coating | Nothing |
| Cutting conditions | Lubrication | Dry |
| | Cutting speed [m/min] | 2.5 and 7.5 |
| | Skew angle [°] | 0 |
| Workpiece | Material | Ti64 |

Tool micro geometry was measured before and after the machining tests by an optical measurement device, Profilometer Alicona IFG4 (see Fig. 3). The setup included a polarized lens of 10x with a ring light to improve the quality of the captured profiles. The vertical resolution was of 200 nm and lateral 2 µm. A cutting edge radius of 10±2 µm was measured in all the edges (see Table 2). No modification of the tool micro geometry due to wear was observed after the broaching tests.

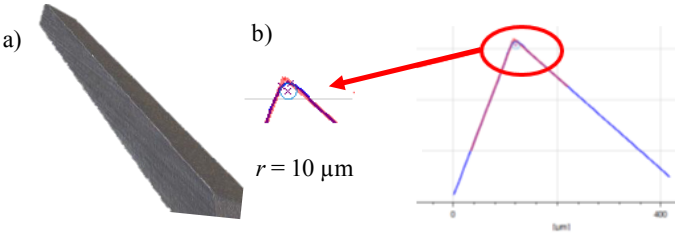


Fig. 3. a) Broaching tooth profile. b) Cutting edge radius.

## 4. Surface integrity characterization

In this section, the methodology followed for the surface integrity characterization of the machined surface is explained. Three main analysis were done: (1) surface topography, (2) residual stresses and (3) material/microstructural damage.

### *4.1. Surface topography*

Two strategies were used to analyze the surface topography of the machined surface. From one side, the portable profilometer Mitutoyo SJ-210 equipment was used to obtain *Ra, Rt* and *Rz* values following the ISO 4287 and 4288. From the other side, the optical profilometer Alicona IFG4 was used to observe the surface topography to identify surface irregularities.

The measurements were carried out not only in the longitudinal direction but also in the transversal one, making at least three measurements for each repetition of cutting condition (see Fig. 2). Hence more than 36 measurements were carried out.

### *4.2. Residual stresses*

The machining-induced residual stresses were measured at the centre of each slot by the hole-drilling technique. The tests were carried out following the procedure given in the ASTM-E837-13 for hole-drilling. As residual stresses generated by machining processes are located in a very shallow layer, the fine increment hole-drilling procedure was followed.

The tests were performed in a Restan MTS3000 machine using a high-speed air turbine and drill bits of 0.8 mm diameter. The incremental hole drilling procedure was carried out at each gauge employing a total of 16 increments in 500 µm depth: (1) first five increments had a depth of 10 µm, (2) the next four 20 µm and (3) the final seven 50 µm.

### *4.3. Material / microstructural damage*

After the residual stresses measurement, each slot was cut longitudinally (in the cutting direction) from the middle of the slot and the machined surface was analyzed by optical microscopy in a Leica DM IRM. Moreover, some of the samples were introduced in the Scanning Electron Microscope (SEM) to make a more detailed analysis of the surface.

## 5. Results and discussion

The results are divided in the different output parameters analyzed, from fundamental variables (forces and chip morphology) to surface integrity aspects (surface topography, residual stresses and microstructural damage). Experimental and FEM results are shown and compared.

### *5.1. Machining forces*

The machining forces from the FEM model were obtained after 2 mm of cut when the thermal steady state was reached. The predicted specific cutting and feed forces (*Ks*) showed good agreement with the experimental results (see Fig. 4). Low deviation was observed in the experimental measurements. Moreover, as expected, the specific cutting and feed forces decreased with the increase of the cutting speed in both approaches, possibly due to the thermal softening of the workpiece.

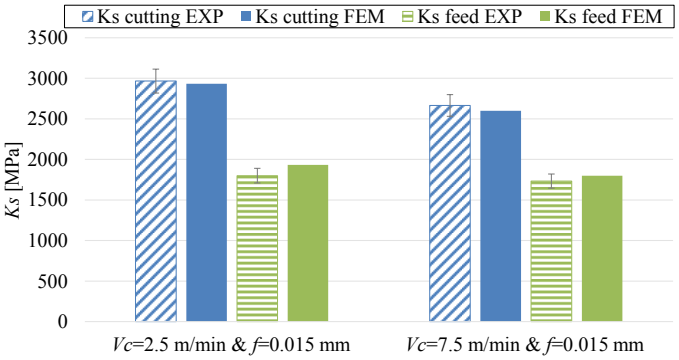


Fig. 4. Specific cutting and feed forces results.

### *5.2. Chip morphology*

Segmented chip was obtained for both cutting conditions due to the material failure criteria. Three parameters were analyzed from each chip: peak, valley and pitch (see Fig. 5). From every test, at least two chips were analyzed and several measurements were done in each of them.

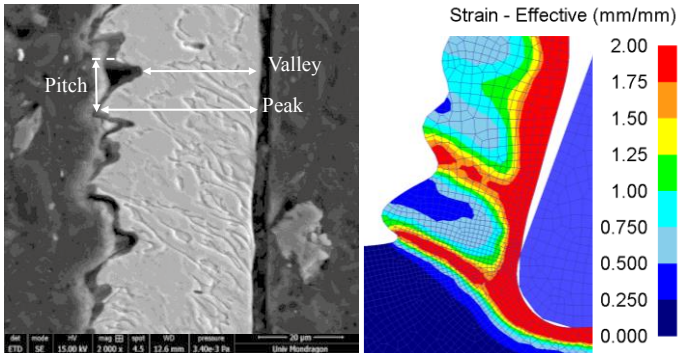


Fig. 5. Chip morphology for *Vc*=2.5 m/min and *f*=0.015 mm.

After all the measurements a comparison between the predicted and the experimental results was done, showing good agreement (see Fig. 6). Nevertheless, higher accuracy was obtained in the peak and valley values in comparison to the pitch distance. The main reason could be a combination of the friction law and the material failure criteria or the experimental process instabilities.

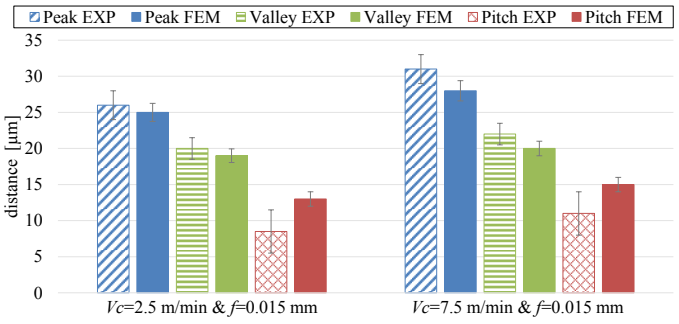


Fig. 6. Chip morphology results.

However, a more in depth analysis was done to observe the strain distribution along the chip. Fig. 5 shows the experimental chip measured by SEM with 2000 magnifications and the FEM results of one of the chips. It was found that in the adiabatic shearing zones accumulation of grains occur, hence, in that zones high deformations arise. In the FEM results high strains values are located also in those areas. Therefore, the model is able to qualitatively represent the strain distribution in the chip.

### 5.3. Surface topography

Fig. 7 shows the roughness results in the transversal and longitudinal direction of the tool travel, measured by the contact profilometer. It was found that increasing the cutting speed, reduces the roughness value in both directions.

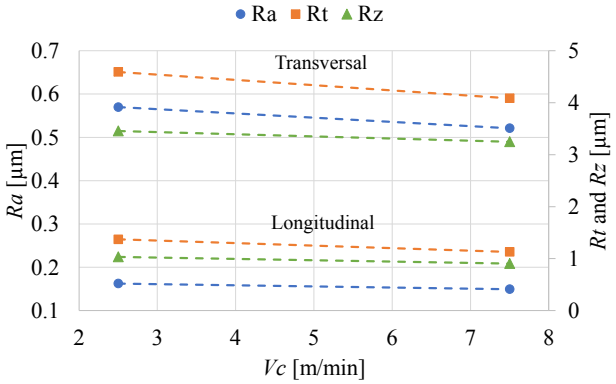


Fig. 7. Roughness results.

Nonetheless, it is remarkable the roughness difference between the longitudinal and transversal direction. Hence, a surface topography analysis was performed by the optical profilometer Alicona IF4. As observed, during the machining process several irregularities were generated along the complete longitudinal direction of the workpiece (see Fig. 8). It should be noted that these irregularities are detected when measuring the roughness in the transversal direction, but not in the longitudinal direction. Probably, these irregularities were associated with the geometrical defects (finishing) of the cutting edge, since, all the machined surfaces had the same marks in the same location.

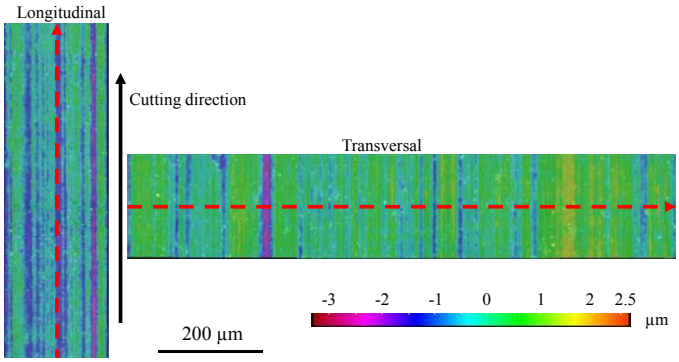


Fig. 8. Surface topography measurements by Alicona IFG4.

### 5.4. Residual stresses

Fig. 9 shows the comparison between the predicted and the experimental results of the residual stresses in the cutting direction. As observed, the prediction follows the experimental trend. The magnitude of maximum compression stress for both cutting conditions is in good agreement with the experimental tests. Nevertheless, the maximum compression stress depth is underestimated for both cutting conditions. Moreover, the stressed layer is also underestimated by the FEM model. The main reason could reside in the thermal properties of the workpiece, since they have not been self-characterized and it is known to be strongly related to residual stresses.

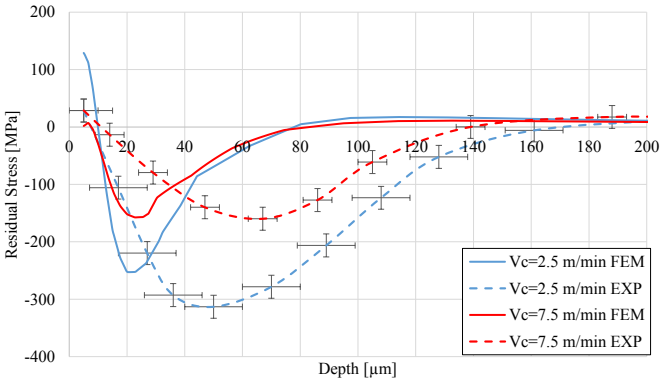


Fig. 9. Residual stresses results.

Nevertheless, the FEM model is able to provide qualitative results and represent the influence of the cutting speed. An increase of the cutting speed from 2.5 to 7.5 m/min produces a reduction in the compression stress peak and in its depth, possibly as a consequence of lower specific forces and therefore lower mechanical effect.

### 5.5. Material / microstructural damage

It was found that when broaching Ti64 a thin layer of disturbed or plastically deformed layer was formed (see Fig. 10). Moreover, in that zone the grains tend to bend down in the cutting direction, producing the orientation of the grains. That phenomena is commonly known as surface drag [11]. Furthermore, it was observed that an increase in the cutting speed seems to produce a slight increase in the affected layer thickness from 5 µm to 8 µm. Considering that the measurement uncertainty is 3.5 µm and the surface drag is not continuous, not clear conclusions could be done up to now.

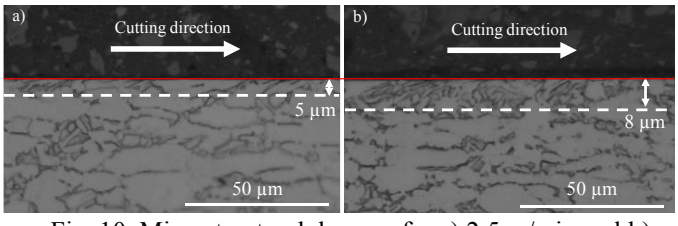


Fig. 10. Microstructural damage for a) 2.5 m/min and b) 7.5 m/min.

Hence, a more in depth analysis of the microstructural damage was done by the SEM equipment. The results conclude that the grains boundaries were deformed in the cutting direction (surface drag) (see Fig. 11). It seems that higher cutting speeds produce a thicker layer of surface drag. However, this conclusion cannot be confirmed yet, as the difference on the thickness of the affected layer is within the range of uncertainty of measurements (3.5 µm) and the phenomena is discontinuous.

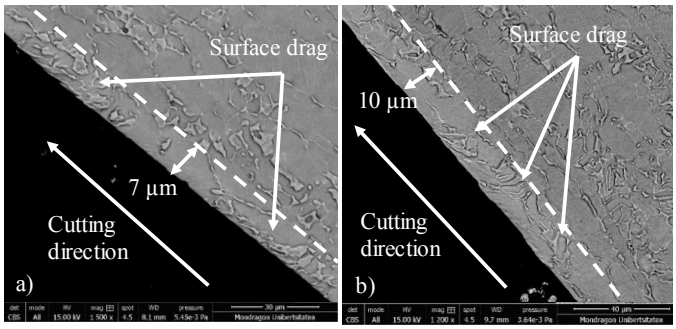


Fig. 11. SEM results of microstructural damage for a) 2.5 m/min and b) 7.5 m/min.

Finally, a comparison between the predicted and the experimental results was done for both cutting conditions. Fig. 12 shows the highest cutting speed results. It was found that in the simulation there was a surface layer of about 8 µm in which the strain values were above 0.8. This qualitatively matches with the experimental results and it is also observed for the lower cutting speed. However, how realistic it is in terms of strain magnitude is not clear from the experimental results.

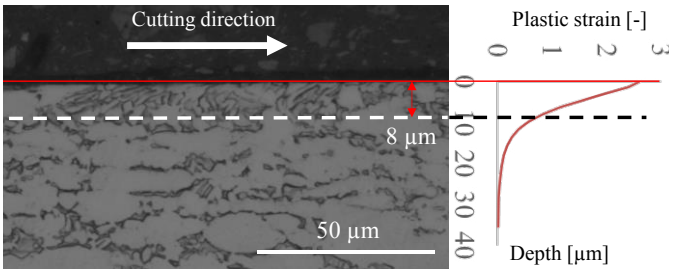


Fig. 12. Experimental and FEM microstructural damage.

## 6. Conclusions

An experimental and FEM analysis of surface integrity when broaching Ti64 has been presented. The main highlights of the study are the following:

- The increase in the cutting speed during the broaching of Ti64 seems to produce an increase in the thickness of the affected layer (discontinuous surface drag), a slight decrease on the surface roughness and an increase in the magnitude of maximum residual compression stress.
- The FEM model is able to predict accurately fundamental variables, such as, cutting forces and chip morphology. Moreover, it is able to reproduce the sensitivity to the cutting speed observed in experimental tests.
- The predictive model is qualitatively accurate in the prediction of residual stresses. Nevertheless, quantitatively significant differences were observed between the prediction and the experimental results in the maximum compression peak depth and the thickness of the stressed layer.
- The FEM model qualitatively predict the material/microstructural damage. Nonetheless, further analysis should be done with more complex material damage and constitutive laws in more severe cutting conditions to observe if the model is able to reproduce the surface plastic strain.

## Acknowledgements

The authors hereby thank the Basque and Spanish Government projects respectively AEROBROCH (UE2016 - 07), GENTALVE (KK-2016/00059), MICROMAQUINTE (PI_2014_1_116), EMULATE (DP12015-67667-C3-3R) and in the grant for Education and Training of Research Staff (PRE_2017_1_0394).

The authors thank the Laboratory Technicians Denis Soriano and Erika Dominguez for their assistance in the realization of experimental tests and surface integrity analysis.

## References

[1] Arrazola PJ, Garay A, Iriarte LM, Armendia M, Marya S, Le Maitre F. Machinability of titanium alloys (Ti6Al4V and Ti555. 3). Journal of materials processing technology. 2009; 209(5): 2223–2230.
[2] M'Saoubi R, Axinte D, Soo SL, Nobel C, Attia H, Kappmeyer G, Engin S, Sim WM. High performance cutting of advanced aerospace alloys and composite materials. CIRP Annals. 2015; 64(2): 557–580.
[3] Courbon C, Pusavec F, Dumont F, Rech J, Kopac J. Tribological behaviour of Ti6Al4V and Inconel718 under dry and cryogenic conditions—Application to the context of machining with carbide tools. Tribology International. 2013; 66: 72–82.
[4] Ulutan D, Ozel T. Machining induced surface integrity in titanium and nickel alloys: A review. International Journal of Machine Tools and Manufacture. 2011; 51(3): 250–280.
[5] Schulze V, Meier H, Strauss T, Gibmeier J. High speed broaching of case hardening steel SAE 5120. Procedia CIRP. 2012; 1: 431–436.
[6] Thakur A, Gangopadhyay S. State-of-the-art in surface integrity in machining of nickel-based super alloys. International Journal of Machine Tools and Manufacture. 2016; 100: 25–54.
[7] Vogtel P, Klocke F, Puls H, Buchkremer S, Lung D. Modelling of process forces in broaching Inconel 718. Procedia CIRP. 2013; 8: 409–414.
[8] Kong X, Li B, Jin Z, Geng W. Broaching performance of superalloy GH4169 based on FEM. Journal of Materials Science & Technology. 2011; 27(12): 1178–1184.
[9] Umbrello D. Finite element simulation of conventional and high speed machining of Ti6Al4V alloy. Journal of materials processing technology. 2008; 196(1-3): 79–87.
[10] Calamaz M, Coupard D, Girot F. A new material model for 2D numerical simulation of serrated chip formation when machining titanium alloy Ti–6Al–4V. International Journal of Machine Tools and Manufacture. 2008; 48(3-4): 275–288.
[11] Childs TH, Arrazola PJ, Aristimuno P, Garay A, Sacristan I. Ti6Al4V metal cutting chip formation experiments and modelling over a wide range of cutting speeds. Journal of Materials Processing Technology. 2018; 255: 898-913.
[12] Arrazola PJ, Özel T, Umbrello D, Davies M, Jawahir I. Recent advances in modelling of metal machining processes. CIRP Annals. 2013; 62(2): 695–718.
[13] Melkote SN, Grzesik W, Outeiro J, Rech J, Schulze V, Attia H, Arrazola PJ, M'Saoubi R, Saldana C. Advances in material and friction data for modelling of metal machining. CIRP Annals. 2017; 66(2): 731–754.
[14] Johnson GR, Cook WH. A constitutive model and data for metals subjected to large strains, high strain rates and high temperatures. Proceedings of the 7th International Symposium on Ballistics. 1983.
[15] Cockcroft M, Latham D. Ductility and the workability of metals. J Inst Metals. 1968; 96(1): 33–39.
[16] Arrazola PJ, Ozel T. Investigations on the effects of friction modeling in finite element simulation of machining. International Journal of Mechanical Sciences. 2010; 52(1): 31–42.
[17] Rech J, Arrazola PJ, Claudin C, Courbon C, Pusavec F, Kopac J. Characterisation of friction and heat partition coefficients at the tool-work material interface in cutting. CIRP Annals-Manufacturing Technology. 2013; 62(1): 79–82.
[18] DEFORM. Deform-User Manual. Scientific Forming Technologies Corporation. 2011